Mercury Cadmium Telluride—A Superior Choice for Near-Room Temperature Infrared Detectors

R. Ashokan and S. Sivananthan
University of Illinois at Chicago, Chicago, IL - 60 607

and

S. Velicu
Smart Pixel Inc., Bolingbrook, IL - 60 440

ABSTRACT

The advantages of mercury cadmium telluride (*HgCdTe*) for hot IR detector applications are discussed. Molecular beam epitaxy (MBE) is used to grow advanced device structures for this purpose. MBE offers the potential to grow *HgCdTe* heterostructure layers on large [7.62 cm (3 in.) or more] silicon substrates leading to very large format and high performance IR focal plane arrays in the future. Preliminary material and device properties achieved in p^+-ν-n^+ device structures grown on 7.62 cm (3 in.) (211)-oriented silicon wafers are discussed.

Keywords: Infrared detectors, mercury cadmium telluride, heterostructures, read-out circuits, molecular beam epitaxy

1. INTRODUCTION

Among a wide range of choice of materials like *HgCdTe*, *InSb*, III-V superlattices (SLs), *InAs/GaInSb* SLs, for IR photon detectors, *HgCdTe* continues to have the largest share of the market. With the development of the cutting-edge molecular beam epitaxy (MBE) technique, *HgCdTe* epilayers can now be grown on 7.62 cm (3 in.) and 10.16 cm (4 in.) silicon substrates[1], overcoming the traditional difficulty in obtaining really large substrates for IR detector array fabrication, particularly based on the exotic *CdZnTe* substrates. The size and density of the manufacturable *HgCdTe* focal plane arrays (FPAs) continues to grow. 1024 x 1024 HgCdTe mid-wavelength infrared (MWIR) FPA has already been demonstrated and 2048 x 2048 is projected in the near future. The requirements of the next generation IR systems include: thermoelectrically (TE) cooled or even uncooled IR FPAs, multispectral/hyperspectral IR FPAs, and advanced simultaneous high resolution and high speed IR imagers. With regard to the compactness, flexibility and system cost, TE cooled, eventually uncooled IR systems will be in great demand. Recent advances have enabled demonstration of portable solid-state imagers operating at room

Revised 18 October 2000

temperature with signal-to-noise ratios of 10 under starlight conditions. Passive low light level imaging applications in the photon-starved MWIR region require simultaneous development of high performance IR devices (TE cooled/uncooled) and the read-out circuit (ROIC) with low input referred noise (typically < 20 electrons) and gateable to support gatewidths of 5 ms or less. To achieve high resolution and high speed simultaneously, integration times much shorter than the state-of-the-art are to be implemented or a radically different approach may be needed to eliminate ROIC, like Rydberg atoms approach[2], where a thin film of Rydberg atoms created by electric field across a cloud of potassium or cesium atoms illuminated by UV laser radiation is used to photoionise the atoms and a set of microchannel plates with phosphor screen and CCD camera are used to capture and display the IR image.

Background-limited performance (BLIP) and high sensitivities at elevated operating temperatures are required for many strategic, space and spectroscopic applications. Currently, the near-room temperature IR photon detectors are sub-BLIP. BLIP operation at f/2 is possible at 115K for *InSb*, and 170K for *HgCdTe* in the MWIR region[3], while the disadvantage of III-V quantum well infrared photodetector (QWIP) due to the very low operating temperature requirement is well known. The advantage of *HgCdTe* is clear. In *HgCdTe*, the fundamental property that limits the operating temperature is the noise due to Auger generation and recombination. Ashley and Elliott[4] proposed the suppression of Auger process by reducing the electron and hole concentrations below their equilibrium values, since the Auger recombination rate is proportional to the square of the carrier concentration. Carrier exclusion in photoconductive devices[5] and carrier extraction in photovoltaic devices[6] have been employed to reduce the carrier concentration in the active volume below their equilibrium level.

To realise the Auger-suppressed devices, an epitaxial process with independent control of composition and doping is critical. Preliminary results on the application of MBE technique to grow *HgCdTe* device structure, particularly to satisfy the low donor doping requirements and the potential for

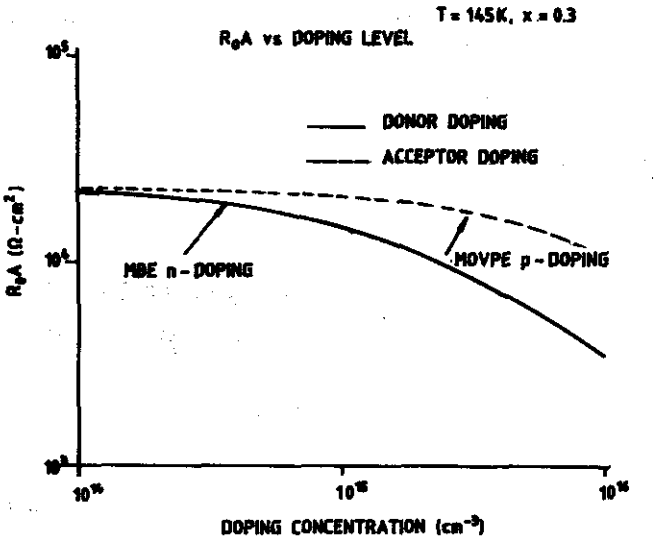

Figure 1. Calculated R_0A as a function of donor or acceptor concentration.

near-room temperature operation of *HgCdTe*-based devices are discussed.

2. DEVICE STRUCTURE SELECTION

Largely based on Tennant and Cabelli[7], the calculations were performed to estimate the theoretical performances. The model assumes that the dominant current is the diffusion from the absorption region. The influence of the interfaces, depletion region and heavily doped side of the junction are neglected. Radiative and Auger mechanism are used for computation of the minority carrier lifetimes. Shockley-Read lifetime is used as an independent input parameter. The ratio of intrinsic Auger 7 to Auger 1 is taken[8] as

$$\gamma = 6\ \{1-5E_g/(4kT)\}/\{1-3E_g/(2kT_g\}$$

The calculated dependence of zero bias resistance-area (R_0A) product on the doping concentration in the two cases of *n* and *p*-type absorber layers is presented in Fig.1. A total carrier extraction was assumed so that Auger and radiative processes are dictated only by the extrinsic doping. It can be seen that a low (10^{14} cm^{-3}) donor doping gives a better R_0A than a 10^{16} cm^{-3} acceptor doping. In practice, it is possible to achieve mid (10^{14}cm^{-3}) donor concentration in the *n*-type absorber layers, while the routinely achievable acceptor concentration in the vacancy or extrinsic-doped *p*-type absorber layer in *HgCdTe* is 10^{16}cm^{-3}.

Two types of configurations ($p\pi n^+$ and n^+vp) are possible to achieve the nonequilibrium mode of operation. It has long been realised that the lifetime in Auger-dominated *HgCdTe* devices is larger in *p*-type material than in *n*-type material, as discussed earlier. Theoretically, as γ is >1 in Eqn (1), higher recombination lifetimes are expected in lightly-doped *p-HgCdTe*. Consequently, $p\pi n^+$ structure is preferable for the near-room temperature operation of nonequilibrium detectors from thermal generation rate point of view. The $p\pi n^+$ structures have been grown by metallo-organic vapour phase epitaxy (MOVPE) and the Auger generation in the π layer was found to be the limiting mechanism[9]. In a recent study, Elliott[10], *et al.*, have shown that the doping required for a background-limited behaviour in MWIR range in a detector with a 2π field-of-view (FOV) is in the mid (10^{14} cm^{-3}) range. Such low *p*-concentrations are hard to achieve in *HgCdTe*. However, MBE technique offers the capability for *n*-type doping in the mid (10^{14} cm^{-3}) range. Indium-doped *n-HgCdTe* with low carrier concentration and low trap density can be routinely grown by MBE [11] whereas, controlling the *p-HgCdTe* doping by incorporating arsenic during MBE technique is still a topic of intense research. Also, the quality of the indium-doped *n-HgCdTe* layers is known to be better than arsenic-doped *p-HgCdTe* layers. This leads to less Shockley-Read centres, increases mobility and excess carrier lifetime. Hence, a structure with good quality *n*-type absorber layer is a practical way to achieve high temperature performance of *HgCdTe*-based devices, though theoretically *p*-absorber, by virtue of longer carrier lifetime, is expected to be better.

This device structure is designed to employ both exclusion at the *nv* contact and extraction at the vp^+ contact, provided the condition for the carrier concentration in the absorber layer is met. However, this triple-layer structure offers an improvement over the conventional double-layer heterojunction (DLHJ) even in the equilibrium mode of operation. In the nonequilibrium mode of operation, near-room temperature, the absorber is intrinsic and the minority carrier extraction occurs at the reverse biased vp^+ junction. The p^+ layer, being wider gap and more heavily doped compared to the absorber layer, the minority carrier hole will not be injected into the absorber layer when this junction is reverse biased. As a result, the net hole concentration in the absorber layer will fall by orders of magnitude. The extraction on the low doped side is even more. On the other hand, the isotype junction (*nv*) forms an excluding hi-lo type of contact to the central absorber region, thus preventing the injection of carriers to replace those extracted at the diode junction. So the minority carrier density drops by several orders of magnitude throughout the central region. It is important to note that since the extraction process is principally a diffusion process, the electric fields are sufficiently low to avoid carrier heating. The reverse bias should be chosen to exceed the critical field necessary for the extraction process, but kept below a certain level to avoid the carrier heating. The required exclusion field can be achieved in the MWIR *HgCdTe* diodes over a wide range of doping levels without exceeding the estimated field for carrier heating.

3. EXPERIMENTAL PROCEDURE

Based on the afore-mentioned discussion, the focus was on p^+vn device structures by MBE. A schematic of such a nonequilibrium photodiode is shown in Fig. 2. The samples generally contain a three-layer heterostructure. Hall measurements were performed to find the carrier concentration and mobility as a function of temperature. The results are shown in Fig. 3 for the first batch of two samples and in Fig. 4 for the next batch of three samples grown by MBE. The structures used here were grown on *CdTe/Si*(211) substrates by MBE. MBE growth chamber was equipped with an *in situ* reflected high energy electron diffraction (RHEED) gun and an ellipsometer to achieve

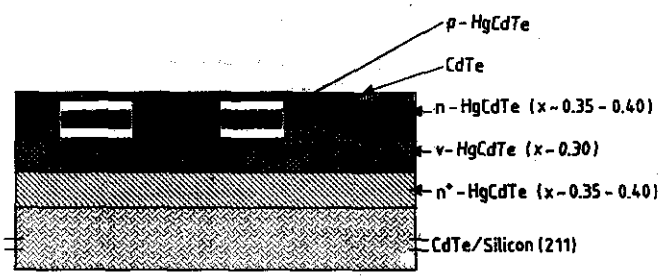

Figure 2. *HgCdTe* heterostructure grown by MBE on silicon (211) substrates.

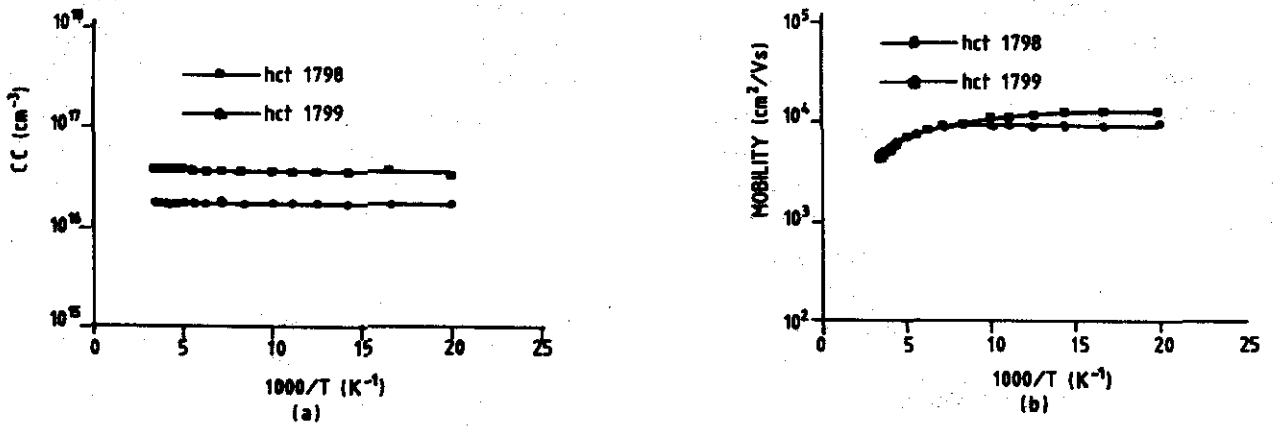

Figure 3. Measured (a) donor concentration, and (b) mobility of the first batch of two samples as a function of temperature after annealing.

real-time monitoring of the crystalline structure and the composition. The *CdTe*(211)/*Si* substrates, with X-ray rocking curve full width at half maximum (FWHM) lower than 100 arc-s and etch-pit densities (EPDs) below 10^5 cm^{-2}, were used for the *HgCdTe* growth. The substrate cleaning schedule used is a well-tested process, whose essential steps are the immersion in a hot trichlorethylene bath, for approx. 10 min, etching in 0.1 per cent *Br-CH_3OH* solution, and multiple rinsing in *CH_3OH*. The nucleation on the *CdTe/Si* substrate was achieved by growing a few monolayers of *HgCdTe*. The targeted structure for this growth consisted of three layers plus a *CdTe* cap layer, as indicated in Fig. 2.

The first *HgCdTe* layer from the top, after the *CdTe* cap is usually a short-wavelength infrared (SWIR) layer. The second layer is a ν-type Indium-doped FWHM MWIR absorber layer, with a targeted *CdTe* mole fraction of 0.3 and a targeted carrier concentration below 2×10^{15} cm^{-3}. The third layer is a heavily indium-doped MWIR layer. After growth, the samples were characterised by FTIR, X-ray rocking curves, and Hall measurements to determine the crystalline and electrical properties.

The structural quality was assessed by measuring FWHM of the X-ray double crystal rocking curve (DCRC). The X-ray rocking curve data were fitted to obtain FWHM of the peaks. From the fitting, the FWHM obtained in the *HgCdTe* layers varied from 100 arc-s to 200 arc-s in the five samples studied, which is typical of *HgCdTe* grown on silicon substrates. Though *HgCdTe* layers grown on lattice-matched *CdZnTe* substrates provides lower FWHM, *HgCdTe/Si* has enormous future potential, particularly for dense and large format FPAs.

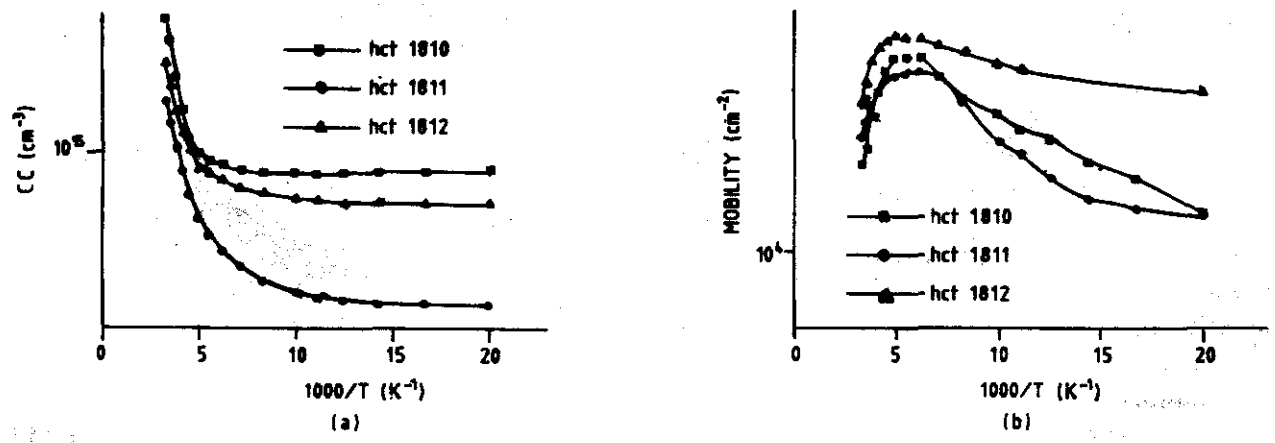

Figure 4. Measured (a) donor concentration, and (b) mobility of the second batch of three samples as a function of temperature after annealing.

Table 1. Summary of the electrical properties of the three samples at 77K

Sample	Carrier concentration (cm^{-3})	Mobility (cm^{-2})	Measured lifetime (μs)	Lifetime (Rad. + Auger theory) (μs)
Hct1810	9.0×10^{14}	17900	1.45	8.5
Hct1811	2.5×10^{14}	14290	2.45	4.0
Hct1812	6.9×10^{14}	24300	2.50	-

Hall effect measurements were carried out at various temperatures after etching away 1 μm of the surface layer and annealing at 235 °C for 12 hr, in a part of each wafer. The temperature dependence of the carrier concentration and mobility are shown in Figs 3(a) and 3(b), respectively, for the first batch and in Figs 4(a) and 4(b), respectively for the second batch of samples studied. The carrier concentration in the absorber in the first batch was higher than the latter samples in the second batch, indicating a continuous improvement in the growth conditions. However, the device results presented here are for samples with higher than the required carrier concentration, thus not yielding the typical negative resistance expected under nonequilibrium operation. Nevertheless, a reasonable responsivity measured at 300K in these devices definitely indicates the feasibility of *HgCdTe*-based IR detectors for near-room temperature operation. Minority carrier lifetime measurements were done by photoconductive decay method on some of the samples. The electrical properties at 77K are summarised in Table 1.

FTIR transmission measurements were performed to determine the thickness of the layers and the composition of the absorber. The data were fit to a multilayer structure model that allows the determination of the thickness of each layer.

3.1 Device Fabrication

The devices were fabricated by standard methods. The *p-n* junction was fabricated by ion implantation followed by a multi-step annealing for arsenic activation and residual mercury vacancy filling. Arsenic ion implantation at 350 KeV and a dose of 10^{14} cm^{-2} and a three-step post-implant annealing as described[12,13] was used to fabricate the planar junction.

4. RESULTS & DISCUSSION

The results of the I-V characteristics at 80K, 150K and 200K for a 40 μm × 40 μm diode is shown in Fig. 5. The R_0A product is 1.1×10^4 Ωcm^2 and the breakdown is in excess of 500 mV. Here, the original *in situ* grown *CdTe* layer is retained as the passivant. However, the previous studies showed that the performance could be improved by removing the *CdTe* cap layer after post-implant annealing and re-passivating the surface. Consequently, the R_0A here is lower than the best results achieved in these kind of devices, resulting also in lower detectivities than expected theoretically[14]. However, in the preliminary effort to study the feasibility of *HgCdTe* on silicon by MBE for high temperature detectors, the results are very encouraging. It is to

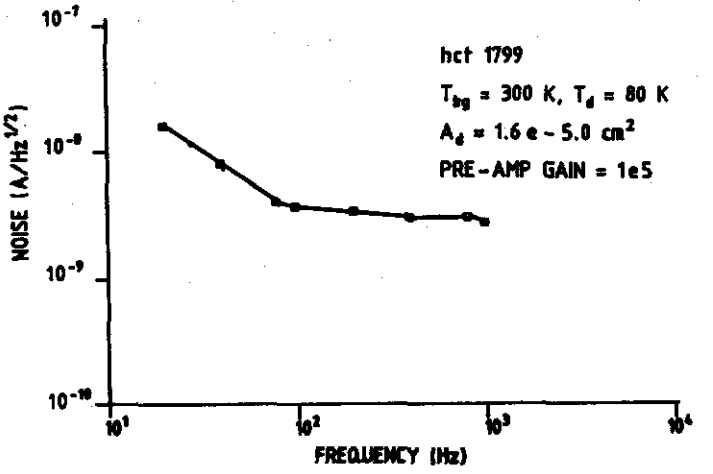

Figure 5. Current-voltage characteristics of a test diode with 40 μm × 40 μm active area at three different temperatures.

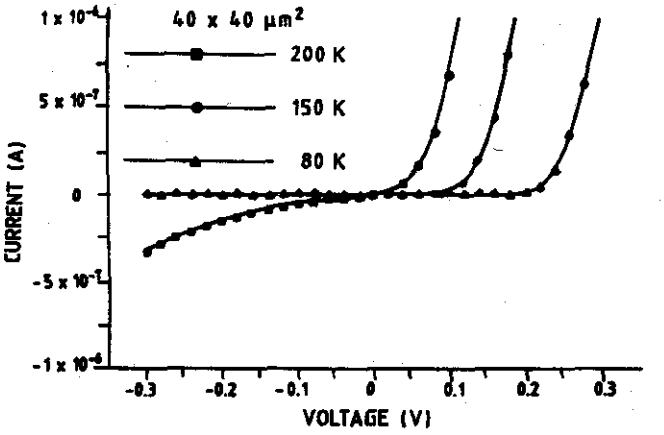

Figure 6. Noise spectrum in log-log scale. The 1/*f* corner frequency is 100 Hz.

be emphasised that the *HgCdTe* on silicon by MBE has a large future potential. Consequently, various user organisations are keen to develop this technology. The forward turn-on voltage decreases with increasing temperature as expected from the band gap dependence on temperature and the breakdown voltage decreases to approx. 400 mV at 200K, in comparison to > 600 mV at 80K.

Responsivity measurement was carried out at 80K and 300K on the same 40 μm × 40 μm diode, using a blackbody at 500K, background temperature of 300K, an aperture size of 0.508 cm (0.2 in.), distance between the blackbody and the detector 12.7 cm (5 in.), and the chopper frequency at 1000 Hz. The measured responsivity was 1.3×10^7 V/W and hence the detectivity was 1.9×10^{11} $cmHz^{1/2}W^{-1}$ at 80K and 1×10^{10} $cmHz^{1/2}W^{-1}$ at 300K. The theoretically expected values are in the range of high (10^{11} $cmHz^{1/2}W^{-1}$) and mid (10^{10} $cmHz^{1/2}W^{-1}$) at 80K and 300K, respectively. The measured noise spectrum at 80K is shown in Fig. 6, which indicates a 1/*f* corner frequency of approx. 100 Hz, slightly higher than the best *HgCdTe* detectors.

Over the past few years, the device structure for Auger suppression has been refined to reduce the minimum current density (J_{min}), to ~10A/cm² at 10 μm cut-off devices[15]. This transforms to a shot noise limited (D^*) of 3×10^9 Jones, an order of magnitude higher than that achieved in pyroelectric devices. However, this D^* cannot be realised in imaging applications due to the high 1/*f* noise levels. The knee frequency (f_k), is of the order 6 MHz in a typical 50 mm diameter, uncooled long-wavelength infrared (LWIR) Auger-suppressed device. For a comparative device at 80K with I_g=14 nA and R_0A = 10 Wcm², the knee frequency is 4 Hz. Obviously, more work needs to be done. The knee frequency, however reduces with decreasing cut-off wavelength. Figure 6 shows the log–log plot of the root mean square (RMS) noise measured as a function of frequency for the device for which I-V is presented in Fig. 5. The measured knee frequency in this device is about 100 Hz at 80K. To reduce the knee frequency, two things are to be done: (i) The total leakage current density has to be reduced, (ii) drastic improvement in passivation is required.

With regard to the former, to realise the full potential of Auger suppression, the Shockley-Read generation needs to be minimised. This can be practically achieved in *n-HgCdTe* layers grown by MBE than *p-HgCdTe* layers, as shown in Fig. 4. High quality *n-HgCdTe* layers with low carrier concentration and low Shockley-Read defect density could be reproducibly grown by MBE[13], while *p-HgCdTe* by arsenic incorporation during MBE growth is still a topic of intense research.

The noise spectrum shown in Fig. 6 is for the same detector for which a detectivity 1.9×10^{11} $cmHz^{1/2}W^{-1}$ at 80K was measured. The noise was measured at zero applied bias and bandwidth 10 Hz. The corner frequency is a function of the leakage current. Lower the leakage current, lower is the 1/*f* knee frequency. In this case, the low 1/*f* knee frequency is consistent with lower leakage current in the devices, as a consequence of lower cut-off wavelength and fairly good electrical properties. As discussed earlier, a typical value for a corresponding LWIR uncooled *HgCdTe* device of 50 μm diameter is 6 MHz, reported by GEC Marconi, UK. Therefore, the current research is focused on reducing the noise in the high temperature *HgCdTe* detectors to make it suitable for imaging applications.

5. CONCLUSIONS

Low donor concentrations of the order 10^{14} cm^{-3} in the absorber layer of the three-layer

HgCdTe heterostructure grown by MBE is demonstrated for the first time. The responsivity 1.3×10^7 V/W, and hence the detectivity 1.9×10^{11} cmHz$^{1/2}$W^{-1} of 40 μm × 40 μm diode at 80K are encouraging. The room temperature detectivity 1×10^{10} cm Hz$^{1/2}$W^{-1} in the p^+-ν-n^+ diode fabricated on *HgCdTe/Si*(211) is a pioneering result. These results indicate that *HgCdTe* is definitely a superior choice for room temperature IR detection. Such a technology developed on 7.62 cm (3 in.) or 10.16 cm (4 in.) *HgCdTe* on silicon substrates is extremely cost-effective with wide application potential.

ACKNOWLEDGEMENTS

This research was carried out under a NASA Contract # NAS5-00096 to Smart Pixel Inc., USA. The technical help from T.S.Lee, P.Boireau, Y.Chen and Z. Ali is greatly appreciated.

REFERENCES

1. Ashokan, R. & Sivananthan, S. *Mater. Sci. Engg.*, 1999, **B67**, 88.
2. *Photonics Technol. News*, July 1999.
3. Kinch, M.A. *J. of Electro. Mater.*, 2000, **29**, 809.
4. Ashley, T.; Elliott, C.T. & Harker, A.T. *Infrared Physics*, 1986, **26**, 303.
5. Ashley, T. & Elliott, C.T. *Electronics. Letters.*,1985, **21**, 451.
6. Rogalski, A. *Optical. Engineering.*, 1994, **33**, 1395.
7. Tennant, W. E. & Cabelli, C. *Mater. Res. Soc. Symp. Proceedings*, 1998, **484**, 221.
8. Casselman, T.N. *J. Appl. Phys.*, 1981, **52**, 848.
9. Elliott, C.T.; Gordon, N.T.; Hall, R.S.; Phillips, T.J.; Jones, C.L.; Matthews, B.E.; Maxey, C.D. & Metcalfe, N.E. *Proceedings SPIE*, 1994, **2269**, 648.
10. Elliott, C.T.; Gordon, N.T. & White, A.M. *Appl. Phys. Lett.*, 1999, **78**, 2881.
11. Shi, X.H.; Rujirawat, S.; Ashokan, R.; Grein, C.H. & Sivananthan, *S. Appl.Phys.Lett.*, 1998, **73**, 638.
12. Ashokan, R.; Dhar, N.K.; Yang, B.; Akhiyat, A.; Lee, T.S.; Rujirawat, S.; Yousuf, S. & Sivananthan, S. *J. Electro. Mater.*, 2000, **29**, 636.
13. Ashokan, R.; Lee, T.S.; Dhar, N.K.; Yoo, S.S. & Sivananthan, S. *Proceedings SPIE*, 2000, **3948**, 63.
14. Lee, T.S.; Ashokan, R.; Grein, C.H.; Yoo, S.S. & Sivananthan, S. *Proceedings SPIE*, 2000, **4028**, 374.
15. Jones, C.L.; Metcalfe, N.E.; Best, A.; Catchpole, R.; Maxey, C.D.; Gordon, N.T.; Hall, R.S.; Colin, T. & Skauli,T. *J. Electro. Materi.*, 1998, **27**, 733.